RESERVOIR STORAGE AND CONTAINMENT OF GREENHOUSE GASES

G.J. WEIR, S.P. WHITE AND W.M. KISSLING

Applied Mathematics, Industrial Research Ltd., P.O. Box 31-310, Lower Hutt, New Zealand

Abstract This paper considers the injection of CO_2 into underground reservoirs. Computer models are used to investigate the disposal of CO_2 generated by an 800 MW power station. A number of scenarios are considered, some of which result in containment of the CO_2 over very long time scales and others result in the escape of the CO_2 after a few hundred years.

1 INTRODUCTION

If atmospheric concentrations of CO_2 are to stabilise without too large an impact on our industrialised lifestyle then novel storage sites for CO_2 are needed. Several researchers (e.g. [Steinburg *et al.*1985], [Ohgaki & Akano1992]) have considered the storage of CO_2 in the oceans, either as a liquid or as a hydrate (approximately $CO_2.6H_2O$). While this approach may be feasible for sources of CO_2 near the coast, costs will be higher for inland areas and an alternative storage technology may be more appropriate. We have investigated an alternative strategy, that of disposing of the CO_2 into deep aquifers within the earth. CO_2 has frequently been injected into petroleum reservoirs for at least two reasons. Some natural gas contains a high proportion of CO_2 and other light hydrocarbons. These may be stripped from the gas stream and reinjected into the reservoir in order to maintain reservoir pressures and to store the remnant hydrocarbons. Injected CO_2 has also been used to enhance oil recovery from low permeability oil reservoirs. The basis of the technology for the injection of CO_2 into aquifers already exists.

This paper describes a preliminary investigation into the storage of CO_2 in deep underground reservoirs. A similar scenario was investigated by [Hendriks *et al.*1991] who suggested the use of exhausted natural gas reservoirs for the storage of CO_2 from natural gas fired thermal power stations. Their paper concentrated on the technology and economics of the power station and recovery of CO_2 from the flue gases and did not examine the storage properties of the reservoir in detail. The emphasis of the current work is the behaviour of the injected CO_2 within the earth and establishing time scales for its return to the atmosphere. While the scenario we investigate is the injection into deep aquifers, the techniques developed would apply equally well if the injection were into a natural gas field. Injection rates considered are consistent with the disposal of the CO_2 generated by a 800 MW thermal power station.

2 MATHEMATICAL BACKGROUND

This section briefly reviews the mathematical equations that describe mass, heat and CO_2 flow in a porous aquifer. The conservation equations for heat, mass and CO_2 are of the form

$$\frac{\partial \rho_\beta}{\partial t} + \nabla . \mathbf{j}_\beta = Q_\beta \qquad \beta = (\text{Energy, Mass}, CO_2) \tag{1}$$

where the density terms and fluxes are given by

$$\begin{aligned} \rho_{CO_2} &= \phi X_l \rho_l S + \phi X_v \rho_v (1-S) \\ \rho_M &= \phi \rho_l S + \phi \rho_v (1-S) \\ \rho_E &= (1-\phi)\rho_m U_m + \phi \rho_l U_l S + \phi \rho_v U_v (1-S) \end{aligned} \tag{2}$$

$$\begin{aligned} \mathbf{j}_{CO_2} &= \rho_l X_l \mathbf{q}_l + \rho_v X_v \mathbf{q}_v \\ \mathbf{j}_m &= \rho_l \mathbf{q}_l + \rho_v \mathbf{q}_v \\ \mathbf{j}_e &= \rho_l h_l \mathbf{q}_l + \rho_v h_v \mathbf{q}_v - K \nabla T. \end{aligned} \tag{3}$$

In these equations ϕ is the porosity, K the rock matrix thermal conductivity, Q_β is a source term, X_α is the mass fraction of CO_2 in phase α =(liquid, vapour), ρ_α is the density of phase α, S is the liquid saturation, U_α is the internal energy of phase α, T is the temperature and P the pressure. The subscript $_m$ refers to the rock matrix.

Table 1: Coefficients of extended Redlick-Kwong EOS

i	1	2	3
c	2.39534×10^{1}	-4.55209×10^{-2}	3.65168×10^{-5}
d	4.09844×10^{-3}	1.23158×10^{-5}	8.99791×10^{-9}
e	2.89224×10^{-7}	8.02594×10^{-11}	7.30975×10^{-13}
f	-6.43556×10^{-12}	2.01284×10^{-14}	-2.17304×10^{-7}

Table 2: Permeabilities used in the simulations

Case	Region			
	Aquifer k_h, k_v	Containment k_h, k_v	Upper k_h	Upper k_v
1a	100 mD	0.01mD	10mD	10mD
1b	100 mD	1 mD	10mD	10mD
5a	100 mD	0.01mD	10mD	2mD
5b	100 mD	1mD	10mD	2mD

The solution of equations (1) is accomplished using a modified version of the computer program TOUGH2 developed at Lawrence Berkeley Laboratories by [Pruess1991].

3 THERMODYNAMIC PROPERTIES OF CO_2

In order to solve the equations of the previous section we need to be able to determine enthalpy, density and viscosity of water-CO_2 mixtures efficiently, for pressures up to 400 bars and temperatures up to 150°C. Equations describing the properties of water at these conditions are readily available (see, for example, [UK Steam Tables1970]).

Previous work on the transport of CO_2 in the earth has been carried out by researchers interested in the effects of non-condensible gases on geothermal fields (e.g. [O'Sullivan *et al.*1985], [Andersen *et al.*1992]). This work did not cover the full pressure range required for the current investigation and new formulae providing accurate approximations to the density, enthalpy and viscosity of CO_2 have either been derived or taken from the literature. These formulae are suitable for describing the properties of CO_2 to a depth of at least 5km. Thermodynamic properties of CO_2 are derived from an extended Redlich-Kwong (RK) equation of state (EOS) ([Kerrick & Jacobs1981]), which provides a good match to experimental values over a wide range of temperatures and pressures. Although it is not necessary for this work, the extended RK equation is easily modified to produce properties of CO_2/water vapour mixtures).

We begin with the extended RK equation of Kerrick and Jacobs and further extend this to provide a better match to properties below 50°C.

$$\frac{P}{\rho} = \frac{RT\left(1+\frac{b\rho}{4}+\left(\frac{b\rho}{4}\right)^2-\left(\frac{b\rho}{4}\right)^3\right)}{\left(1-\frac{b\rho}{4}\right)} - \frac{c(T)+d(T)\rho+e(T)\rho^2+f(T)\rho^3}{\sqrt{T}\,(b+\rho^{-1})} \tag{4}$$

where $b = 5.8\times10^{-5}\text{m}^3/\text{mole}$ and $c(T) = c_1 + c_2T + c_3T^2$. $d(T), e(T)$ and $f(T)$ are defined in a similar manner. Coefficients c_j etc. are given in table 1. The work of Kerrick and Jacobs does not have the f(T) term. Most of the required properties of CO_2 can be derived from the EOS given by equation (4).

Fugacity

The fugacity of CO_2 (f) can be derived from the EOS given in equation 4 by the expression ([Prausnitz1969])

$$RT\,log(f) = \int_v^\infty (P - \frac{RT}{v})dv - RT\,log(Z) + RT(Z-1) \tag{5}$$

Here Z is the compressibility factor given by $Z = \frac{RT}{PV}$. Evaluating equation (5) with the EOS given in equation (4) leads to

$$\begin{aligned}\log(f) &= \frac{8y-9y^2+3y^3}{(1-y)^3} - \log(Z)\\ &- \frac{c(T)}{RT^{3/2}(v+b)} - \frac{d(T)}{RT^{3/2}v(v+b)} - \frac{e(T)}{RT^{3/2}v^2(v+b)} - \frac{f(T)}{RT^{3/2}v^3(v+b)}\\ &+ \frac{c(T)\log(v/(v+b))}{RT^{3/2}b} + \frac{d(T)\log((v+b)/v)}{RT^{3/2}b^2} - \frac{e(T)\log((v+b)/v)}{RT^{3/2}b^3}\\ &- \frac{f(T)\log(v/(v+b))}{RT^{3/2}b^4} - \frac{d(T)}{RT^{3/2}bv} - \frac{e(T)}{RT^{3/2}2bv^2} + \frac{e(T)}{RT^{3/2}b^2v}\\ &- \frac{f(T)}{RT^{3/2}3bv^3} + \frac{f(T)}{RT^{3/2}2b^2v^2} - \frac{f(T)}{RT^{3/2}b^3v}\end{aligned} \tag{6}$$

where $y = \frac{b\rho}{4}$, $v = \frac{1}{\rho}$ and $c(T), d(T), e(T), f(T)$ are as defined in equation (4).

The enthalpy of CO_2 is determined through the use of residual properties. A residual fluid property is defined as the difference between a real fluid property and the perfect gas state property value. We follow the procedure described in [Patel & Eubank1988]. The residual enthalpy is given by:

$$H - H^*_{ref} = H(T,\rho) - H^*\left(T_{ref}, P_{ref}/RT_{ref}\right)$$

where * indicates the perfect gas state.

Integration is done along the path

$$H\left(T,\rho_e\right) \to H^*(T,0) \to H^*\left(T_{ref},0\right) \to H^*\left(T_{ref}, \frac{P_{ref}}{RT_{ref}}\right)$$

Starting with the thermodynamic identity

$$dU = C_v dT + R\left(\frac{\partial Z}{\partial(1/T)}\right)\frac{d\rho}{P\rho}$$

the residual internal energy is calculated using

$$\frac{U - U^*_{ref}}{RT} = \frac{1}{T}\int_0^{\rho}\left(\frac{\partial Z}{\partial(1/T)}\right)\frac{d\rho'}{\rho'} + \frac{1}{T}\int_{T_{ref}}^{T}\frac{C^*_v}{R}dT \tag{7}$$

This allows the residual enthalpy to be calculated as

$$\frac{H - H^*_{ref}}{RT} = \frac{U - U^*_{ref}}{RT} + Z - \frac{T_{ref}}{T}$$

We use the same reference state as in [Patel & Eubank1988]: $U^*_{ref} = -RT_{ref}$, $H_{ref} = 0$, $P_{ref} = 10^6$ Pa and $T_{ref} = 273.16°K$. The integrals in equation 7 require an integration of the perfect gas properties as well as integration of terms derived from the EOS given in equation (4). [Sweigert *et al.*1946] give the formula

$$C_p = 16.2 - \frac{6.53\times10^3}{T} + \frac{1.41\times10^6}{T^2}$$

for the specific heat at constant pressure (units are BTU/(lb-mole)/ °R) of CO_2 at zero pressure. Converting this to MKS units and noting that for a perfect gas $C_p = C_v + nR$, where n is the number of moles, allows us to write

$$\int_{T_{ref}}^{T}\frac{C^*_v}{R}dT = 59.315\left(T - T_{ref}\right) - 15139.5\left(\log\left(\frac{T}{T_{ref}}\right)\right) - 1808600\left(\frac{1}{T} - \frac{1}{T_{ref}}\right)$$

where T is in °K.

The first integral in equation 7 is rather long and has been evaluated using the symbolic algebra package MAPLE. For completeness we give the result here.

$$\begin{aligned}
\textstyle\int_0^{\rho}\left(\frac{\partial Z}{\partial(1/T)}\right)\frac{d\rho'}{\rho'} &= (log(b\rho+1)(b^3(18c_1 + 6c_2T - 6c_3T^2) + b^2(-18d_1 - 6d_2T + 6d_3T^2)\\
&+ b(18e_1 + 6e_2T - 6e_3T^2) + (-18f_1 - 6f_2T + 6f_3T^2))\\
&+ b^3\rho^3(6f_1 + 2Tf_2 - 2T^2f_3) + b^3\rho^2(9e_1 + 3Te_2 - 3T^2e_3)\\
&+ b^2\rho^2(-9f_1 - 3Tf_2 + 3T^2f_3) + b^3\rho(18d_1 + 6Td_2 - 6T^2d_3)\\
&+ b^2\rho(-18e_1 - 6Te_2 + 6T^2e_3) + b\rho(18f_1 + 6f_2T - 6f_3T^2))\\
&\quad (12RT^{5/2}b^4)^{-1}
\end{aligned}$$

Fortunately MAPLE may also be used to generate FORTRAN (or C) code and this was done to produce subroutines to calculate the thermodynamic properties of CO_2.

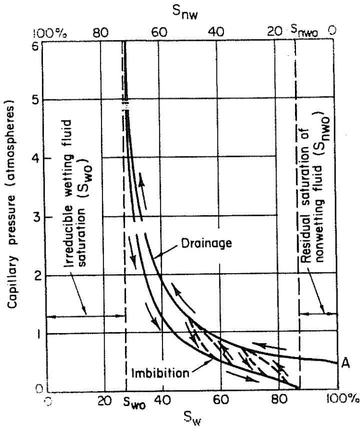

Figure 1: Typical capillary pressure - liquid saturation curves.

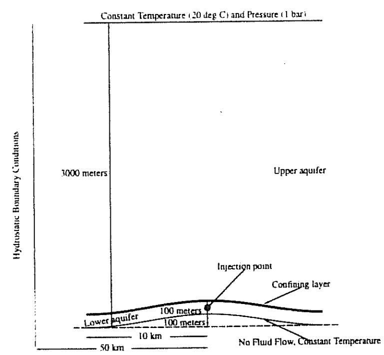

Figure 2: Portion of a generic reservoir used in modelling

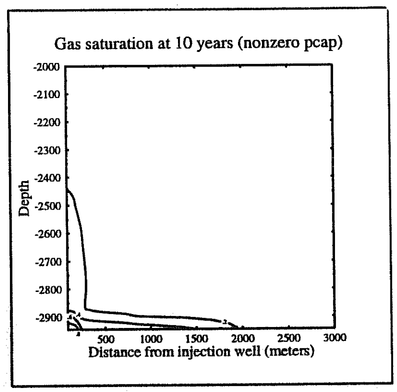

Figure 4: Gas saturation at 10 years, pcap=0

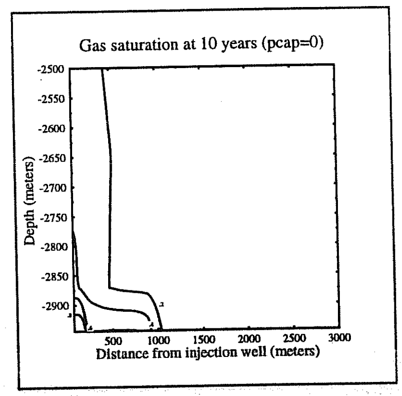

Figure 3: Gas saturation at 10 years, nonzero pcap

When considering the containment of a gas by a capping structure over a permeable reservoir an important property of the capping structure is the capillary pressure function. Experimentally, capillary pressure displays hysteretic behaviour such as that sketched in figure 1 (taken from Bear (1972)). The existence of a non-zero vapour entry pressure means that a capping structure can trap a layer of gas, typically a few tens of meters thick, beneath it. With a zero vapour entry pressure this trapping does not occur (although the escape of gas may be extremely slow when the capping structure has low permeability).

For the work described here we have ignored the hysteretic nature of capillary pressure but have included a non-zero vapour entry pressure. The functional form of capillary pressure chosen for this work is taken from Varva et al. (1992) and we have fitted a curve of the form $P_c = 1.08 \times 10^{-3}\sqrt{\frac{\phi}{k}}10^F$ where $F = 1.031(4.58 - 7.75S_l + 8.22S_l^2 - 3.40S_l^3)$. to the experimental data presented for "rock3" in figure 6 of [Varva *et al.*1992] (scaled to represent CO_2 - water rather than mercury - air).

5 PARAMETER SELECTION

The gross topography of subsurface layers of the earth is well known in many areas of the world. Seismic prospecting for petroleum reservoirs has resulted in reasonably detailed knowledge of the underground layered structure, especially in sedimentary basins. Regions where underground layering is convex upwards (anticlines) are natural sites for entrapment of petroleum products and these are also natural sites for storing greenhouse gases. The results of petroleum exploration, whether successful or not, provide a ready made database of suitable sites for the disposal of carbon dioxide. The type of trap modelled in this study consists of an almost impervious cover or cap rock overlying a permeable rock aquifer. A cross-section through the reservoir geometry considered in this paper is illustrated in figure 2.

We choose as an injection rate 100 kg/sec and assume this is all into a single well. This is representative of the CO_2 produced by a 800 MW thermal power station. Hendriks et.al. argue that an injection rate of about 10 kg/sec is a realistic average value for injection into depleted natural gas reservoirs. Experience in reinjecting waste water into geothermal fields suggests our higher value may be achievable in some aquifers.

6 SIMULATIONS AND RESULTS

All of the simulations performed in this report assumed an initial hydrostatic state consistent with the

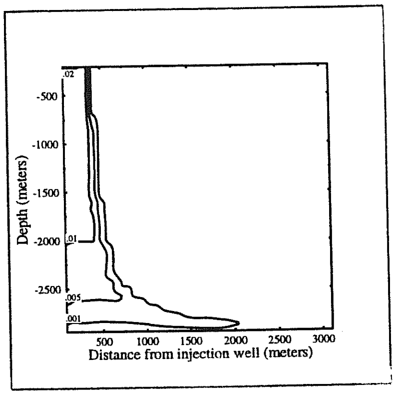

Figure 5: Gas saturation at 1000 years, pcap=0

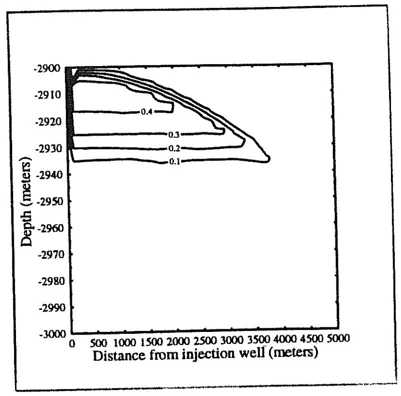

Figure 6: Gas saturation at 5000 years, nonzero pcap

for obtaining the initial conditions was set at 3100 m depth, to be below the undulating lower aquifer, and had a fixed temperature of 113° C. By permitting only heat flow (zero mass flow) across this lower boundary, and running the model for about 10^{13} seconds, a satisfactory quasi-steady state was obtained. This resulted in a pressure at the lower boundary of about 324 bars.

Four different permeability structures were assumed in the simulations. Table 2 lists the permeabilities used in the different simulations. Here k_h and k_v refer to the horizontal and vertical permeabilities. Corey (1977) relative permeability functions were used, with $S_{rg} = 0.05$, and $S_r = 0.3$. In all cases the rock porosity is taken as 0.1 in the upper and lower aquifers, and 0.04 in the confining layer. CO_2 is injected into the lower aquifer at 100 kg/s for 10 years and the simulation is continued to a total time of 5000 years.

We will consider the results of a single case (Case 1b) with and without capillary pressure effects in some detail, the results are similar to the other cases considered, although some CO_2 escapes to the atmosphere in Case 1b and it can be considered a "worst case " scenario.

Figures 3 (zero capillary pressure) and 4 (nonzero capillary pressure) show contours of gas saturation in a small section of the reservoir near the injection point immediately after injection has ceased. The differences in the saturation contours for these two cases can be quite clearly seen. When capillary pressure is included more gas is contained beneath the confining layer. This remains the case for the whole of the period of the simulation.

In figure 5 we show saturation contours after 1000 years for the case of ignoring capillary pressure and in figure 6 we show saturation contours after 5,000 years including capillary pressure. In the latter case most of the CO_2 is contained as a gas beneath the confining layer while in the former case the gas has reached the surface. This behaviour is also illustrated in figures 8 and 7.

The variation of location of CO_2 in these figures requires some explanation. The mechanism for the transport of CO_2 to the upper aquifer then back to the lower is the same in both cases. Initially as the gas is injected, a single phase bubble of gas forms. this is surrounded by a two-phase zone containing CO_2 and water saturated with CO_2. Buoyancy forces cause the bubble and surrounding two-phase zone to rise towards the surface. This upward movement towards the surface is delayed when capillary pressure is included until the gas pressure is sufficient to overcome the vapour entry pressure of the confining layer. Almost immediately injection is ceased the single phase gas bubble collapses into a two-phase area.

Liquid water saturated with CO_2 at reservoir conditions considered here is slightly more dense than pure water. The CO_2 saturated water sinks down towards the lower aquifer drawing more pure water towards the two-phase zone. Effectively CO_2 gas is washed from the two-phase zone and carried to the lower aquifer in the dense CO_2 saturated liquid. The liquid flows associated with this are shown in figure 9.

When capillary pressure is not included some gas does escape to the atmosphere, however most of the gas is contained dissolved in the liquid phase. This contrasts to the case when capillary pressure is included and almost all of the CO_2 is contained as a gas in a two-phase zone.

7 CONCLUSIONS

These research results show that underground storage of greenhouse gases is an attractive option, being:

- Self-containing. Results from the computer model show that provided the CO_2 is initially spread hori-

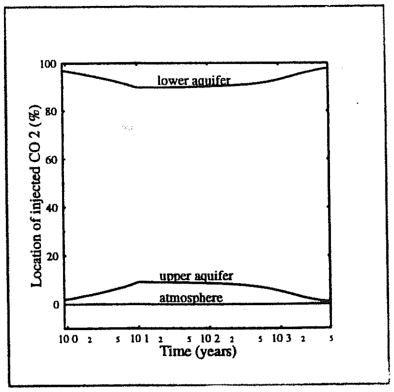

Figure 7: Disposition of CO_2 at 5000 years, nonzero pcap

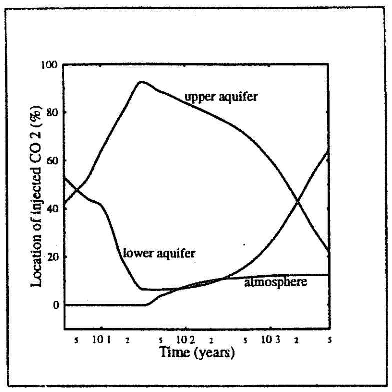

Figure 8: Disposition of CO_2 at 5000 years, pcap=0

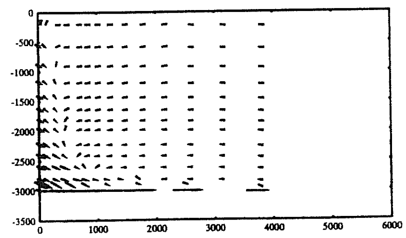

Figure 9: Liquid velocity vectors at 1000 years, pcap=0

- Volumetrically efficient. The greenhouse gases are stored at densities of hundreds of kilograms per cubic metre for several hundred years. Upward migration and dissolution reduces the storage density to about 40 kg/m^3 over about one thousand years. However, a non-zero vapour entry pressure term could significantly increase the density of the stored greenhouse gases.
- Viable. Aquifer permeabilities of 100 mD were assumed in our model calculations. Such permeabilities should exist within many geologic formations.

7 ACKNOWLEDGEMENT

This work was sponsored by New Energy and Industrial Technology Development Organisation (NEDO) / Research Institute of Innovative Technology for The Earth(RITE) of Japan.

*

References

Andersen, G. Probst, A. Murray, L. Butler, S., An Accurate PVT Model for Geothermal Fluids as Represented by $H_2O - CO_2 - NaCl$ Mixtures, *Proc. 17th Workshop on Geothermal Reservoir Engineering*, Stanford University, Jan 1992.

Bear, J., *Dynamics of fluids in porus media.* American Elseveir Publishing Company, Inc. 1972

C.A. Hendriks, K. Blok and W.C. Turkenburg, *Energy - The International Journal* 16,1277-1293 1991.

D.M. Kerrick and G.K. Jacobs, A Modified Redlich-Kwong Equation for H_2O, CO_2 and $H_2O - CO_2$ mixtures at Elevated Temperatures and Pressures, *Amer. J. Sci.* **281**, 1981.

K. Ohgaki and T. Akano, *Energy and Resources* 13,375-383, 1992.

O'Sullivan, M.J. Bodvarsson, G.S. Pruess, K. Blakeley, M.R. : 1985, Fluid and Heat Flow in Gas-rich Geothermal Reservoirs *Soc. Pet. Eng. J.* **Vol. 25** pp 215-225

Patel, M.R. Eubank, P.T. :1988, Experimental Densities and Derived Thermodynamic Properties for Carbon Dioxide-Water Mixtures *J. Chem. Eng. Data* **Vol. 33** pp 185-193

Prausnitz, J.M. :1969, *Molecular Thermodynamics of Fluid-Phase Equilibria* Englewood Cliffs, New Jersey, Prentice Hall Inc. p41

Pruess, K. (1991), TOUGH2 - A General-purpose numerical simulator for multiphase fluid and heat flow., *Report LBL-29400, Lawrence Berkeley Laboratory.*

M. Steinburg, H.C. Cheng and Horn, *A system study for the removal, recovery and dispossal of carbon dioxide from fossil fuel plants in the US*, Brookhaven National Laboratory 1985.

Sweigert, R.L. Weber, P. Allen, R.L. :1946, Thermodynamic Properties of Gases: Carbon Dioxide *Ind. & Eng. Chem.* **Vol 38**

UK Steam Tables in SI Units :1970, Edward Arnold London

Varva, C.L. Kaldi, J.G. Sneider, R.M., Geological Applications of Capillary Pressure: A Reveiw, *The Amer. Assn. Pet. Geol. Bull.*, **Vol 36** pp840-850 1992.